Global Minimum Structures of Morse Clusters as a Function of the Range of the Potential: $81 \leq N \leq 160$

Longjiu Cheng and Jinlong Yang*

Hefei National Laboratory for Physics Sciences at Microscale, University of Science and Technology of China, Hefei, Anhui 230026, People's Republic of China

Received: March 21, 2007; In Final Form: April 19, 2007

We have attempted to find the putative global minimum structures of Morse clusters for cluster size $N = 81-160$ as a function of the range of the potential (with potential range $\rho_0 \geq 3.0$). Moreover, compared to the results for $N \leq 80$ listed in the Cambridge Cluster Database, a number of new putative global minima are given. A structural and conformational analysis of M_{100} for different ρ_0 was given. The sequences of the global minima as a function of ρ_0 and N were studied, and the zero temperature "phase diagram" was given for an overall view of how the global minima depend upon N and ρ_0.

1. Introduction

Structural information is of great importance for many chemical and physical fields. In the past 20 years, developing an efficient structural optimization method to find the low-energy or ground-state structures of atomic/molecular clusters has attracted great interest.[1−13] Compared to bulk materials, the ground-state (or global minimum) structures of clusters are always very novel, e.g., the fullerene clusters,[14] the cage- and cubic-like water clusters,[15,16] and the hollow cage-like Au clusters.[17,18]

The electronic structure determines the ground-state geometric structure, but generally, it's too expensive to have a systematic global geometric optimization directly using a quantum mechanics (QM) method. Alternatively, model and empirical potentials are largely used to fit the interactions among particles, and the results are generally acceptable in a certain precision compared to the experiments or QM methods.

For various clusters, the range of the interaction is a key parameter determining the ground-state structures, e.g., at small cluster size, for sodium clusters with a long-ranged interaction, disordered and icosahedral motifs are most favored;[19] for the Lennard-Jones (LJ) clusters with a middle-ranged interaction, icosahedral motifs are most favored and only at some magic numbers decahedral, face-centered cubic (fcc), and tetrahedral motifs can be global minima;[16] and for C60 molecular clusters with a very short-ranged interaction, decahedral, tetrahedral, and close-packed motifs are predominant.[20,21]

Morse potential[22] can be taken as a test system with pair interaction

$$V(r) = \epsilon \cdot e^{\rho_0(1-r/r_e)}[e^{\rho_0(1-r/r_e)} - 2]$$

where ϵ is the pair well depth, r_e is the equilibrium distance, and the parameter ρ_0 determines the potential range; larger ρ_0 means more short-ranged interaction. Using the Morse potential, Doye et al.[23,24] have had a systematic study about how the range of the potential affects the global minimum structures. They located putative global minimum structures as a function of the range of the potential ρ_0 and gave out the structural phase diagram for cluster size $N \leq 80$.

In this work, we try to locate the putative global minimum structures of Morse clusters as a function of ρ_0 for slightly larger cluster sizes ($81 \leq N \leq 160$) using the newly developed dynamic lattice searching (DLS)[11] method. Moreover, for $N \leq 80$, a number of new global minimum structures are located.

2. Computational Method

DLS combines advantages of the lattice searching method and the stochastic unbiased global optimization method, and has been proved to be an efficient unbiased cluster optimization method for the optimization of LJ clusters and C60 molecular clusters.[11,21] Moreover, DLS can locate the lowest-energy structures of various motifs (e.g., icosahedral, decahedral, and close-packing) instead of only the global minimum one.[25] To have a systematic study on the global minimum structures of Morse clusters as a function of the range of the potential, at each ρ_0 among 3.0, 3.5, 4.0, 4.5, 5.0, 6.0, 8.0, 10.0, and 14.0, 10^4 DLS runs were carried out separately, and the 20 lowest-energy minima located in the DLS runs for each ρ_0 were recorded. Finally, the putative global minimum structures for potential range $\rho_0 \geq 3.0$ are found out from the recorded minima.

3. Results and Discussion

3.1. Conformational and Structural Analysis of M_{100}. To have an understanding of the funnel information of the energy landscape and structural information for various packing styles, a conformational and structural analysis of Morse clusters with atom number $N = 100$ (M_{100}) is given, where we think that, approximately, a motif with higher hit number is more predominant in conformation and lies in a wider funnel on the energy landscape.[25] Figure 1 plots the conformational distribution of M_{100} during 10^4 DLS runs at $\rho_0 = 3.0$, 3.5, 4.5, 6.0, 8.0, and 14.0. Structures labeled in Figure 1 are classified by the motifs: disordered (dis), Mackay icosahedral (I), I plus anti-Mackay overlayers (I+), distorted I+ (*I+), polyicosahedral (PI), decahedral (D), D plus anti-Mackay overlayers (D+), tetrahedral (T), face-centered cubic (fcc), and close-packed (cp).

* Corresponding author. Tel: +86-551-3606408. Fax: +86-551-3602969. E-mail: jlyang@ustc.edu.cn.

10.1021/jp072238g CCC: $37.00
Published on Web 05/24/2007

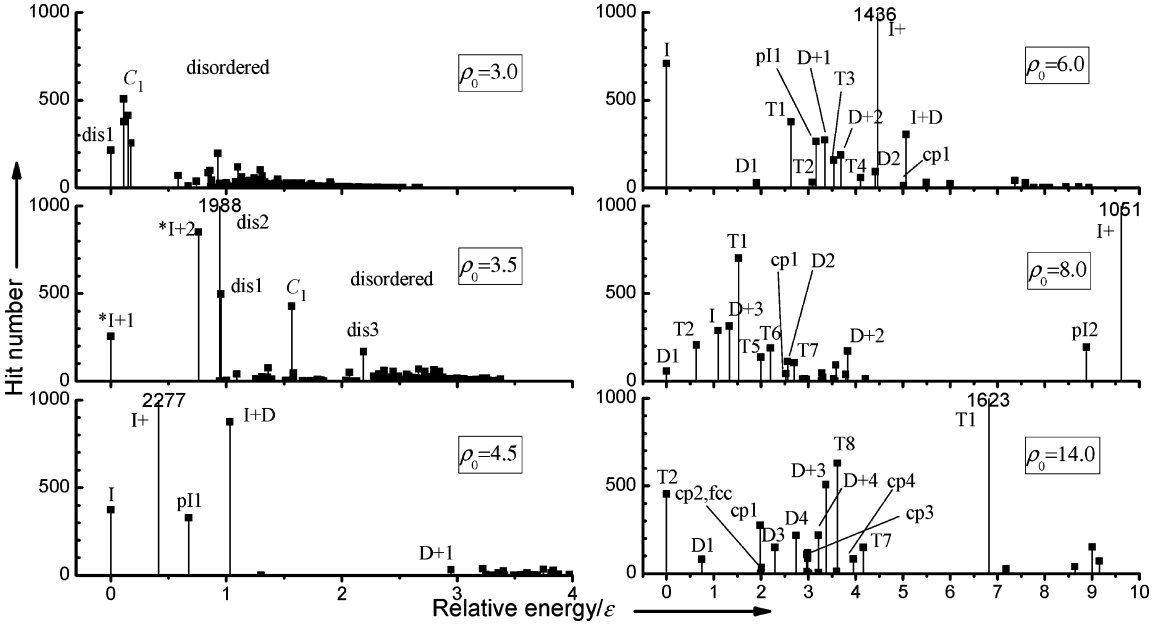

Figure 1. Structural distributions of M_{100} clusters in 10^4 DLS runs for $\rho_0 = 3.0$, 3.5, 4.5, 6.0, 8.0, and 14.0 (as labeled). The *y*-axis gives the hit numbers of various metastable local minima during the 10^4 DLS runs. The *x*-axis gives relative energy from the global niminum structure. The hit numbers out of range are labeled in the figure. The indexes of each motif are also labeled.

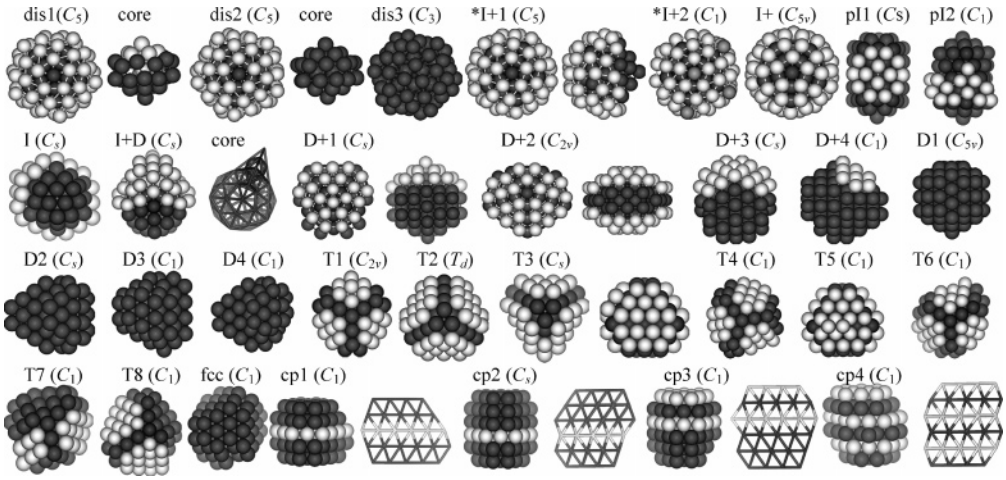

Figure 2. Various structures of M_{100} as labeled in Figure 1. Enclosed are the point groups. For some cases two sides of views are given, and the sites are given in different shades to show the topological structure more clearly.

The basic structural categories of the ordered packing are I, D, T, fcc, and cp, where the maximal coordination number of one atom is 12. fcc cluster is a fragment of fcc crystal and can be contained in an fcc tetrahedron. I is packed by 12 tetrahedrons sharing one common vertex. D is packed by 5 tetrahedrons sharing one common edge. T has a tetrahedral core and may have outer tetrahedrons sharing the four {111} faces of the core. T, fcc, and cp can be strain-free. PI is packed by I motifs sharing the five top tetrahedrons. The labeled structures are plotted in Figure 2.

At $\rho_0 = 3.0$, most of the located structures are disordered, and the global minimum structure (dis1) has a distorted 39-atom icosahedral core and a regular tight outer shell, which is somewhat similar to the polyicosahedral core−shell clusters.[26] At $\rho_0 = 3.5$, disordered clusters are energetically in disfavor relative to distorted I+ clusters (*I+1 and *I+2), but still are predominant in conformation and have most hit numbers, where dis2 is similar to dis1 but its core is more like a distorted 39-atom decahedral cluster. At $\rho_0 = 4.5$, icosahedral clusters (I, I+, PI1, and I+D) become predominant in both energy and conformation. *I+1 is distorted I+ both in the surface and in the core to have more nearest neighbors, and can be transformed to I+ after relaxation at $\rho_0 = 4.5$. PI1 and PI2 can be thought as polyicosahedron,[27] but are based on the 55-atom Mackay icosahedron (Ih55). The core of I+D is a union of icosahedron and decahedron. At $\rho_0 = 6.0$, I still is the global minimum and I+ is most predominant in conformation, but the energetic gap between I and I+ increases and the energetic gaps between I and decahedral or tetrahedral clusters decrease. D1, D2, D3, and D4 are decahedral motifs; D+1, D+3, and D+4 are decahedra plus anti-layers on one side of {111} faces; D+2 is decahedron plus anti-layers on both sides of {111} faces. T1 is the 98-atom Leary tetrahedron[28] plus two atoms (based on the 4-atom edged tetrahedron); T2 is based on the 6-atom edged tetrahedron; T3, T4, T5, T6, T7, and T8 are based on the 5-atom edged tetrahedron. T2, fcc, cp1, cp2, cp3, and cp4 are both strain-free clusters,[29] but T2 has stacking faults in four directions of {111} layers, fcc has no stacking fault, and cp1, cp2, cp3, and cp4 have stacking faults in only one direction of {111} layers. At $\rho_0 = 8.0$, D1 becomes the global minimum structure, but I+ still is the most dominant conformation despite its high energy. At $\rho_0 = 14.0$, T2 is the global minimum, icosahedral

TABLE 1: New Putative Global Minimum Structures at $N \leq 80$[a]

N	PG	motifs	NN	E_{strain}	$\rho_0 = 3.0$	$\rho_0 = 6.0$	$\rho_0 = 10.0$	$\rho_0 = 14.0$	ρ_{min}	ρ_{max}
10a	D_{2d}	2D+	26	0.0859	−30.825058	−26.588332	−25.960250	−25.840646	17.023	
11a	C_{3v}	dis	31		−37.886544				3.491	3.676
24a	C_s	2PI	88	6.7627	−124.498381	−89.415307	−81.585755		8.225	8.933
26a	C_s	2PI,I+	98	9.6577	−142.361067	−99.545037	−88.715128		7.678	7.995
29a	C_s	2I+	113		−167.108031	−113.549356			6.802	6.975
29b	C_s	4D	103	0.2458		−111.513973	−103.947386	−102.744078	11.061	11.207
32a	D_{3h}	3T,D+	117	0.9434	−188.968428	−125.863078	−117.237209	−115.432942	10.083	11.537
33a	C_s	2PI,I+	134		−202.101265	−131.893912			5.725	5.745
34a	C_s	3I	128	3.6247	−209.830547	−136.524962	−125.552036		8.278	8.579
36a	C_s	2I+	152		−230.198460	−145.144166			4.499	4.854
38a	C_3	dis	156		−247.324804	−155.568927			4.544	4.937
39a	C_5	3I″	153		−255.643276				4.389	4.742
40a	D_{6h}	dis,2PI	171		−265.425496	−166.008623			4.108	5.025
41a	D_3	dis	171		−273.570563	−170.187434			4.547	4.553
41b	C_s	dis,2PI	175		−273.338612	−170.327675			4.553	4.708
42a	C_s	dis,2I+	178		−285.119843	−174.062576			4.469	4.597
43a	C_s	dis,2I+	186		−295.132688	−179.076290			4.333	4.448
44a	C_{2v}	dis,2PI	191		−302.767757	−184.833284			4.174	4.831
44b	C_s	3I	175	5.6110	−303.600375	−187.344244	−171.111366		9.000	9.399
45a	C_s	dis,2PI	198		−314.407214	−188.034882			4.129	4.212
45b	C_s	dis,2PI	195		−312.722886	−189.721433			4.212	4.502
46a	C_s	dis,2PI	204		−325.144128	−191.683099			3.750	4.073
47a	C_1	dis,2PI	204		−335.821344	−196.410327			3.719	3.838
47b	C_2	dis,2PI	209		−334.272064	−198.601793			3.838	4.185
47c	C_s	dis,2PI	208		−333.023153	−198.813474			4.185	4.262
48a	C_s	dis	214		−346.662788	−200.030314			3.242	3.861
48b	C_s	dis	212		−343.696158	−204.298868			3.861	4.216
49a	C_5	dis	213		−355.522137	−207.617845			3.840	3.929
50a	C_s	3I	204	9.1289	−363.380857	−219.163495	−197.123775		3.890	4.937
51a	C_s	dis	231		−376.631334	−218.675700			3.385	3.758
51b	C_1	3I	210	8.5744		−225.210338	−203.624838	−194.956337	7.144	7.425
53a	C_s	4T	212	0.8191		−232.060537	−213.889957	−210.925799	10.297	10.308
56a	C_s	dis	258		−428.496002	−243.948769			3.363	3.615
57a	C_{2v}	3I+″	247		−436.630741				3.908	4.533
57b	C_{2v}	3I+	240	10.5469		−257.604126	−231.988382	−219.551585	4.533	4.752
57c	C_s	3I+	241	10.7118		−257.950515	−232.709814	−220.265507	4.752	5.028
58a	C_{2v}	dis	254		−447.812676	−257.048479			3.978	4.074
58b	C_s	3I+″	246	10.5660		−261.950240	−235.992154	−223.520289	4.074	4.102
59a	C_s	3I+″	251	10.5884	−453.831656	−267.348139	−241.012509	−228.486823	4.260	4.858
62a	C_{2v}	dis	288	11.8708	−490.743003	−276.056534			3.107	4.514
62b	C_1	3I+″	265	11.5713		−283.133335	−255.155600	−241.815901	4.514	4.657
63a	C_1	dis	291		−501.276459				3.213	3.446
63b	C_s	dis	291		−500.208115	−281.303611			3.446	4.334
64a	C_{3v}	dis	299		−510.627671	−285.009129			3.376	4.343
65a	C_1	dis	304		−520.878839	−289.921751			3.510	4.225
66a	C_1	dis	310		−531.877652	−294.567339			3.457	4.228
66b	C_s	3I+	286	13.5437		−303.262241	−272.373110	−257.984208	4.228	4.255
67a	C_1	dis	313		−542.476797	−299.701936			3.505	4.068
67b	C_s	3I+	289	15.7649		−308.913158	−276.158986		4.114	5.196
68a	C_s	dis	318		−554.981243	−302.707317			3.335	3.438
68b	C_1	dis	319		−554.520713	−303.557452			3.438	3.451
68c	C_s	dis	321		−553.363223	−303.577887			3.451	3.951
68d	C_1	3I+″	297			−312.642581			3.951	4.184
68e	C_s	5D	283	0.5643		−311.231888	−286.246653	−282.604561	11.514	12.484
69a	C_1	dis	327		−565.907867	−308.764626			3.301	3.426
69b	C_s	dis	326		−565.630050	−308.817610			3.426	3.568
69c	C_{2v}	dis	316		−563.961350	−311.375984			3.568	3.874
69d	C_1	3I+″	303		−562.944706	−318.459290			3.874	4.35
70a	C_1	dis	335		−577.286914	−313.273673			3.216	3.461
70b	C_1	dis	331		−576.341992	−314.187108			3.461	3.736
70c	C_5	3I+″	309		−572.226257	−324.143464			3.736	3.954
70d	C_1	3I+″	309	11.3497	−571.752458	−324.370120			4.136	4.16
71a	C_s	dis	349		−588.345014	−319.253314			3.020	3.025
71b	C_s	dis	345		−588.332142	−316.248223			3.025	3.189
71c	C_s	dis	332		−587.953339	−318.473867			3.189	3.298
71d	C_s	dis	329		−587.599409	−318.515013			3.298	3.69
72a	C_1	dis	352		−599.406547	−322.142169			3.067	3.078
72b	C_s	dis	344		−599.297191	−322.716667			3.078	3.45
72c	C_s	dis	345		−599.049445	−323.356172			3.450	3.704

TABLE 1: (Continued)

N	PG	motifs	NN	E_{strain}	$\rho_0 = 3.0$	$\rho_0 = 6.0$	$\rho_0 = 10.0$	$\rho_0 = 14.0$	ρ_{min}	ρ_{max}
72d	C_2	dis,I+	325		−595.063785	−331.393629			3.704	3.816
72e	C_1	3I+″	321		−595.064909				3.816	4.052
73a	C_s	dis	349		−610.843103				3.015	3.823
73b	C_1	3I+″	325		−606.917536				3.824	3.858
73c	C_1	3I+″	325		−605.468812				3.858	4.108
74a	C_1	3I+″	330		−617.864423				3.881	3.972
74b	C_1	3I+″	329		−618.802036				3.972	4.033
75a	C_s	dis	357		−632.435998				3.225	3.855
75b	C_1	3I+″	335		−629.796590				3.856	4.011
75c	C_1	3I+	328	18.9564	−627.536328	−350.984741	−312.486515	−295.888665	4.011	5.003
76a	C_s	dis	368		−643.984157				3.225	3.403
76b	C_1	dis	364		−643.111552				3.403	3.868
76c	C_1	3I+″	333	19.9633	−641.116800	−355.850733	−316.498615		3.868	4.276
77a	C_s	dis	368		−653.480087				3.438	3.732
77b	C_1	3I+″	345		−652.186718				3.732	4.139
78a	C_s	dis	392		−667.519832				3.154	3.435
78b	C_s	dis	376		−664.936478				3.435	3.637
78c	C_1	3I+″	351		−663.138941				3.637	3.932
79a	C_1	dis	400		−678.920223				3.185	3.399
79b	C_1	dis	378		−678.786959				3.399	3.427
79c	C_1	dis	382		−677.838383				3.427	3.493
79d	C_2	3I+″	357		−674.451312				3.493	4.005
80a	C_1	dis	403		−690.518910				3.041	3.15
80b	C_1	dis	407		−690.458744				3.151	3.332
80c	C_1	dis	384		−690.053940				3.332	3.418
80d	C_1	dis	387		−689.067555				3.418	3.488
80e	C_1	3I+″	363		−685.686196				3.488	4.024

[a] PG gives the point group. NN gives the nearest-neighbor contacts. ρ_{min} and ρ_{max} give the range of ρ_0 for which the structure is the global minimum. E_{strain} gives the strain energy at $\rho_0 = 10.0$. All energies are given in units of the pair well depth, ϵ. If the structure is unstable, no value of energy is given. The motifs are classified by the packing styles (see ref 25), and the "″" means the structure is distorted.

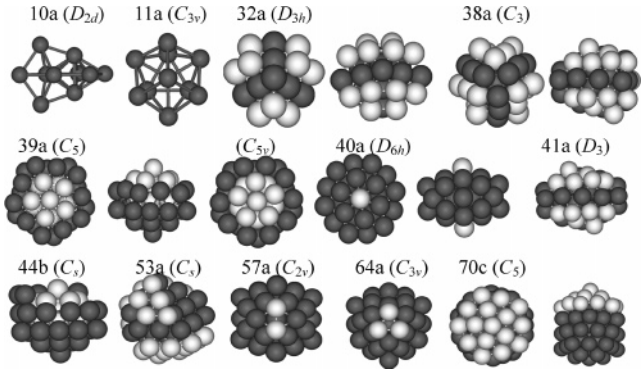

Figure 3. Some typical structures of the newly located global minimum at $N \leq 80$.

structures are unstable, and the energy of T1 increases much but becomes the most predominant conformation.

3.2. New Global Minimum Structures at $N \leq 80$. Morse clusters for cluster size $N \leq 80$ have been systematically studied by various global optimization methods,[23,24,29−31] and the global minimum structures are available online from the Cambridge Cluster Database (CCD).[16] To check with the results in CCD, we also optimized Morse clusters at $N \leq 80$, and found out a number of new putative global minimum structures for a certain range of ρ_0 as listed in Table 1.

Most of the new global minima are disordered clusters or distorted icosahedral clusters and similar to the structures given in CCD. Some typical or novel structures given in Table 1 are plotted in Figure 3: 10a is polydecahedral; 11a is disordered; 32a is tetrahedral (based on the 3-atom edged tetrahedron); 38a is disordered; 39a is distorted icosahedral, where the {100} faces are distorted to {111} faces to have more nearest-neighbors; 40a is the magic 38-atom polyicosahedron[26,27] plus two vertices; 41a is 38a plus three atoms; 44b is icosahedral; 53a is tetrahedral (based on the 4-atom edged tetrahedron); 57a is Ih55 plus two atoms and little distorted; 64a is the magic 61-atom T_d[27] plus three atoms; 70c is one-vertex missed Ih55 plus a regular distorted anti-layer cap.

3.3. Global Minimum Structures at $81 \leq N \leq 160$. To further investigate the relationship between the global minimum structures and the range of the potential at larger cluster sizes, we located the putative global minima of Morse clusters at $81 \leq N \leq 160$ with potential range $\rho_0 \geq 3.0$.[32] For $\rho_0 < 3.0$, the potential is too long-ranged, so we think it may be unreasonable for real systems.

At the middle-ranged potential, icosahedral clusters are predominant in potential energy. Figure 4 plots some typical icosahedral minima: 83E, 89F, 92E, 99E, 116C, 135B, and 137E are Ih55 plus various incomplete regular Mackay overlayers; 81F, 85C, 88C, 95D, 106E, 115B, and 127C are Ih55 plus regular anti-Mackay overlayers, 156F is 6-vertices missed Ih147 plus a regular anti-Mackay cap and little distorted, and 157F is Ih147 plus anti-Mackay overlayers; 81E, 88B, 106D, 115A, and 127A are distorted 81F, 88C, 106E, 115B, and 127C, respectively, but unlike 85C, 85B is 3-vertices missed Ih55 plus distorted anti-Mackay overlayers; 87E is a magic number Ih55-based polyicosahedron, and 101F, 111F, and 152G are 87E plus regular anti-layers. The distorting can make the isosahedral clusters more strained but, on the other hand, more compact and have more nearest-neighbors. Therefore, at small ρ_0 (about smaller than 4.0), the distorting of icosahedral clusters may decrease the potential energy.

At very small ρ_0, due to the very strong long-distance interaction, there are many packing styles to make the structures more compact and spherical. These packing styles are called disordered packing, where the coordination number of one atom

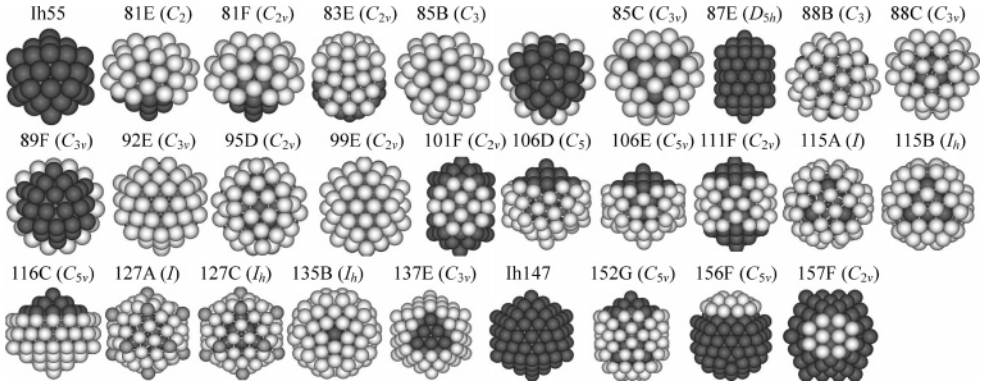

Figure 4. Global minima of Morse clusters with icosahedral packing.

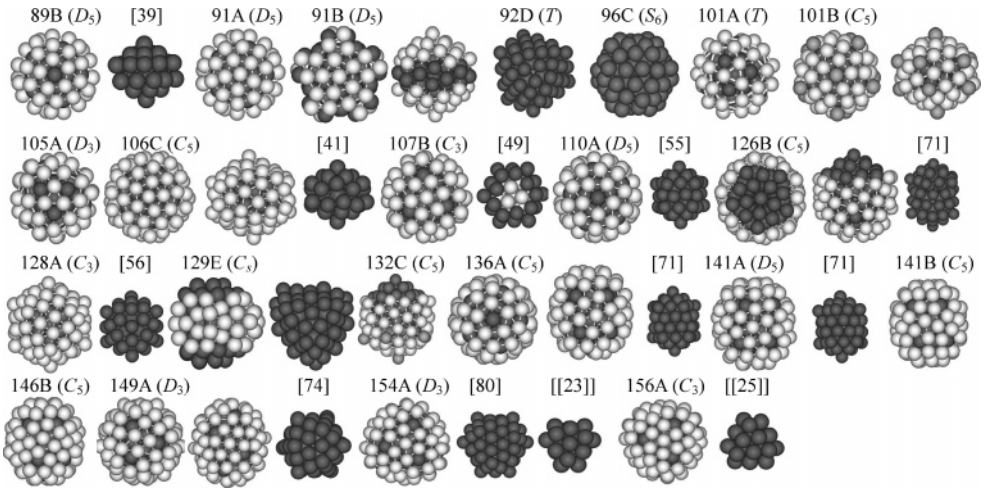

Figure 5. Global minima of Morse clusters with disordered packing. The numbers enclosed by "[ ]" are the size of the core.

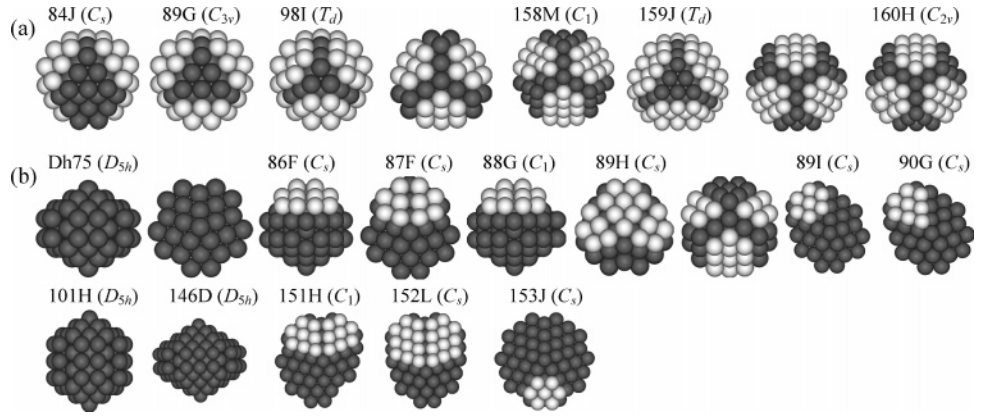

Figure 6. Global minima of Morse clusters with (a) tetrahedral packing and (b) magic number Marks decahedral packing or decahedral packing with anti-layers.

may be larger than 12. Figure 5 plots the magic numbers of the distorted clusters: 89B, 91A, and 101B are a 39-atom core plus compact outer shells; 91B is a distorted decahedron plus two distorted caps; 92D is similar to a rearrangement of the icosahedral 92E and is known as the global minimum of sodium clusters;[32] 96C has a very strange symmetry (S_6); 101A and 105A are largely compressed core plus spherical outer shells; 107B is the 49-atom icosahedron (one {111} face missed Ih55) plus a compact outer shell; 110A has a 55-atom core which is a little-distorted ordered isomer of Ih55; 126B, 132C, 136A, 141A, 141B, and 146B are a 71-atom icosahedral core plus various outer shells (the distorting styles may be different); 106C, 128A, and 149A both have largely distorted core to make the structures spherical enough; 129E is similar to an Ih55-based polyicosahedron (in three directions); 154A is the 23-atom icosahedron plus two layers of outer shells, and 156A is similar to 154A but the core is 25-atom disordered. Most magic numbers of the distorted global minima are core−shell clusters; i.e., an ordered core (icosahedral or decahedral, may be little distorted) plus a spherical outer shell, where the packing styles of the core and the outer shell are different. The icosahedra plus complete anti-Mackay overlayers (115A, 115B, 127A, and 127C) are also core−shell clusters. Core−shell clusters can be sufficient spherical and compact, and so are favored for the very long-ranged potentials.

At very large ρ_0, the potential is very short-ranged, so icosahedral clusters become too strained, and the global minima are close-packed or decahedral clusters, which have been sufficiently discussed in the literatures.[29,33] However, between the middle- and short-ranged potential (near $\rho_0 = 8.0$), we found

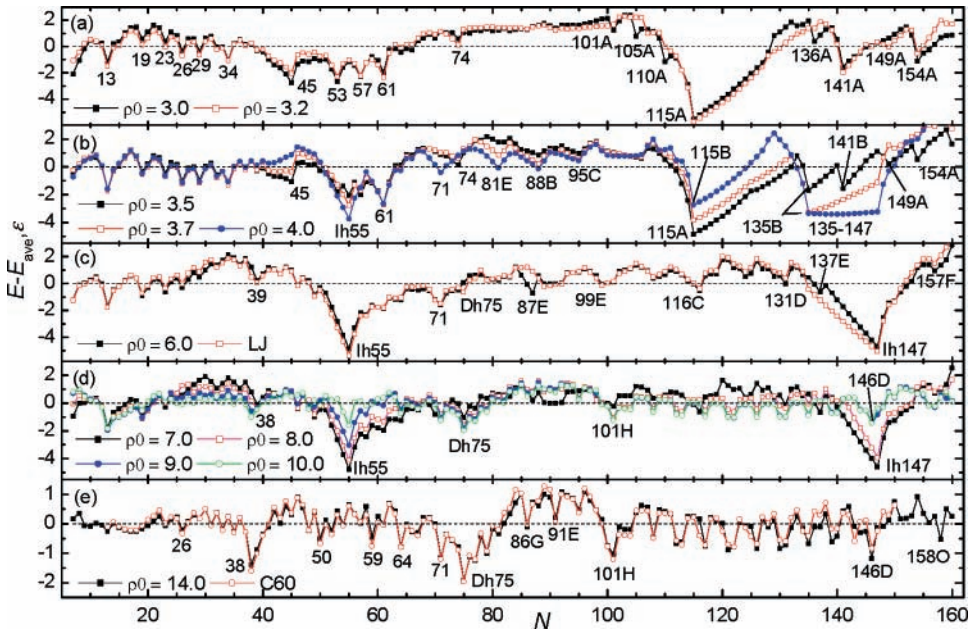

Figure 7. Plots of the energies of the global minima as a function of cluster size $10 \leq N \leq 160$ for various clusters (as labeled). E is the energy of the global minima, and E_{ave} is a four-parameter fit of the global minima. Downward peaks represent the most stable magic numbers compared to the neighbors. Data of LJ clusters are from the CCD,[16] and data of C60 molecular clusters are from ref 21.

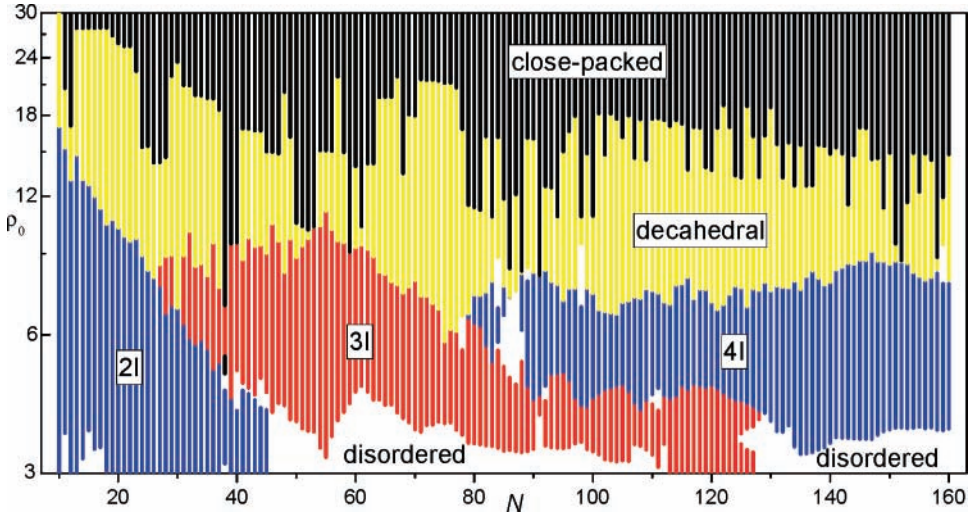

Figure 8. Zero temperature "phase diagram" showing the variation of the lowest-energy structure with N and ρ_0. Labeled are the structural types: close-packed, decahedral, icosahedral (2I, 3I, and 4I), and disordered, where 2I is based on Ih13, 3I is based on Ih55, and 4I is based on Ih147 (may be incomplete or have anti-layers). The distorted icosahedra are included in the area of icosahedral motifs, while the polyicosahedra are not included.

some Leary tetrahedron-like[28] global minima. As shown in Figure 6a, 98I is the Leary tetrahedron, 89G is 98I minus a cap, 84J is 89G minus a patch, 159J is the next magic number of Leary tetrahedron (based on the 5-atom edged tetrahedron), 158M is 159J minus one atom, and 160H is 159J plus one atom. Moreover, there are also some global minima with decahedral packing plus anti-Mackay overlayers (D+). As shown in Figure 6b, each of the D+ global minima has a rather regular anti-Mackay cap or surface, where 89H is most interesting, which seems like both D+ and tetrahedral motifs.

3.4. Sequence Analysis of the Global Minima. Figure 7 plots the sequences of the energy of the global minima at various ρ_0 to find out the most stable magic numbers. First, as shown in Figure 7a, for the very long-ranged potential ($\rho_0 = 3.0$, 3.2), at $N > 80$, the most stable structures are the core−shell clusters (101A, 105A, 110A, 115A, 136A, 141A, 149A, and 154A). The magic number Ih45 is also a core−shell cluster which has an Ih13 core and a complete anti-Mackay outer shell. Second, Figure 7b shows that, with ρ_0 increasing ($\rho_0 = 3.5$, 3.7, and 4.0), peaks of the core−shell magic numbers gradually disappear or become weaker, and the icosahedral magic numbers (Ih55, 71, 81E, 88B, 95C, 135−147) appear, where Ih55 and 135−147 are Mackay icosahedra (I), while 71, 81E, 88B, 95C, 115A, and 115B are Ih55 plus various anti-Mackay overlayers (I+, may be little distorted). 135B is the 12-vertices missed Ih147, which is more spherical, and so is more dominant than Ih147 at smaller ρ_0. Next, Figure 7c compares the energetic sequences of Morse clusters at $\rho_0 = 6.0$ and the LJ clusters, which shows that the sequences of the two potentials have very similar outlines except for very few cases (Dh75, 87E, and 137E). Morse potential at $\rho_0 = 6.0$ and the LJ potential are very similar near the curve bottom, and the difference is that the interaction of Morse potential is too weak at long distances. Dh75 has fewer nearest-neighbor contacts (NN) compared to relative icosahedral clusters (I) but is more spherical, so it has stronger non-NN interactions and favors more the potentials with stronger long

distance interaction. 137E is the one-face missed Ih147, which also has large NN but is less spherical and so favors more the Morse potential. 87E is the polyicosahedral (PI) cluster, which has similar NN with relative I+ motifs but is much less spherical than relative I+ or I motifs, and so it is even not the global minimum for LJ clusters. However, 87E is less strained than relative I+ motifs and has more NN than relative I motifs, so it acts as a magic number for Morse clusters at $\rho_0 = 6.0$. Then, as shown in Figure 7d, with ρ_0 increasing ($\rho_0 = 7.0$, 8.0, 9.0, and 10.0), peaks of the icosahedral magic numbers (39, 71, Ih55, 87E, 116C, and Ih147) gradually disappear, and peaks of decahedral or fcc magic numbers (38, Dh75, 101H, and 146D) appear but are weaker than those of the icosahedral magic numbers at smaller ρ_0. Last, Figure 7e plots the sequences of the Morse clusters at $\rho_0 = 14.0$ and the C60 molecular clusters with the Girifalco potential,[34] which are both clusters with very short-ranged potentials. For a short-ranged potential, NN is most important in determining the potential energy; i.e., isomers with the same NN and same packing style (decahedral or close-packed) will have very similar potential energy. Therefore, it can be seen that the two clusters have very similar energy sequences of the global minima, although the motifs of the global minima may be different.

Figure 7 shows that, with ρ_0 increasing, the sequences of the most stable magic numbers are disordered core−shell clusters, icosahedral clusters, decahedral and close-packed clusters. Finally, to give an overall view of how the global minima depend upon N and ρ_0, following Doye et al.,[23,24] Figure 8 plots the zero temperature "phase diagram" for $10 \leq N \leq 160$, and $\rho_0 \geq 3.0$. With ρ_0 increasing, structural transition may be disordered to icosahedral, icoshahedral with anti-layers to icoshahedral without anti-layers (2I to 3I, and 3I to 4I), icosahedral to decahedral, decahedral to close-packed, and icosahedral directly to close-packed (38−40, 59, and 91). The blanks between 2I and 3I are disordered structure (e.g., 38a, 40a, and 41a as shown in Figure 3), the blanks between 3I and 4I are the Ih55-based polyicosahedra (e.g., 87E as shown in Figure 4), and the blanks between icosahedral and decahedral are the Leary tetrahedron-like structures (as shown in Figure 6a).

4. Conclusions

In conclusion, with the dynamic lattice searching (DLS) method, we have attempted to find the putative global minimum structures of Morse clusters for cluster size $N \leq 160$ as a function of the range of the potential (with potential range $\rho_0 \geq 3.0$), which is notoriously difficult for unbiased global optimization methods. Compared to the results for $N \leq 80$ listed in the Cambridge Cluster Database (CCD), a number of new putative global minima were given. We studied the structural and conformational distribution of M_{100} for different ρ_0 to know about the funnel information of the energy landscape. The sequences of the global minima as a function of ρ_0 and N were studied, and the zero temperature "phase diagram" was given to find out how the global minima depend upon N and ρ_0. The global minima of Morse clusters can act as a structural bank, which may be helpful in determining the global minimum structures of other atomic or molecular clusters.

Acknowledgment. This work is partially supported by the National Natural Science Foundation of China (50121202, 20533030, 10474087), by the National Basic Research Program of China (2006CB922004), by the USTC-HP HPC project, and by the SCCAS and Shanghai Supercomputing Center. L.J.C. gratefully acknowledges the support of the K. C. Wong Education Foundation, Hong Kong.

Supporting Information Available: Table of the global minima of Morse clusters at $81 \leq N \leq 160$. This material is available free of charge via the Internet at http://pubs.acs.org.

References and Notes

(1) Northby, J. A. *J. Chem. Phys.* **1987**, *87*, 6166.
(2) Xue, G. L. *J. Global Optim.* **1994**, *4*, 425.
(3) Deaven, D. M.; Ho, K. M. *Phys. Rev. Lett.* **1995**, *75*, 228.
(4) Wales, D. J.; Doye, J. P. K. *J. Phys. Chem. A* **1997**, *101*, 5111.
(5) Romero, D.; Barrón, C.; Gómez, S. *Comput. Phys. Commun.* **1999**, *123*, 87.
(6) Hartke, B. *J. Comput. Chem.* **1999**, *20*, 1752.
(7) Locatelli, M.; Schoen, F. *Comput. Optim. Appl.* **2002**, *22*, 175.
(8) Johnston, R. L. *J. Chem. Soc., Dalton Trans.* **2003**, *22*, 4193.
(9) Lee, J.; Lee, I. H.; Lee, J. *Phys. Rev. Lett.* **2003**, *91*, 080201.
(10) Cheng, L. J.; Cai, W. S.; Shao, X. G. *Chem. Phys. Lett.* **2004**, *389*, 309.
(11) Shao, X. G.; Cheng, L. J.; Cai, W. S. *J. Comput. Chem.* **2004**, *25*, 1693.
(12) Takeuchi, H. *J. Chem. Inf. Model.* **2006**, *46*, 2066.
(13) Baletto, F.; Ferrando, R. *Rev. Mod. Phys.* **2005**, *77*, 371.
(14) Kroto, H. W.; Allaf, A. W.; Balm, S. P. *Chem. Rev.* **1991**, *91*, 1213.
(15) James, T.; Wales, D. J.; Hernández-Rojas, J. *Chem. Phys. Lett.* **2005**, *415*, 302.
(16) Wales, D. J.; Doye, J. P. K.; Dullweber, A.; Hodges, M. P.; Naumkin, F. Y.; Calvo, F.; Hernández-Rojas, J.; Middleton, T. F. The Cambridge Cluster Database (CCD), available from http://www-wales.ch.cam.ac.uk/CCD.html.
(17) Li, J.; Li, X.; Zhai, H. J.; Wang, L. S. *Science* **2003**, *299*, 864.
(18) Johansson, M. P.; Sundholm, D.; Vaara, J. *Angew. Chem., Int. Ed.* **2004**, *43*, 2678.
(19) Noya, E. G.; Doye, J. P. K.; Wales, D. J.; Aguado, A. *Eur. Phys. J. D* (in press).
(20) Doye, J. P. K.; Wales, D. J.; Branz, W.; Calvo, F. *Phys Rev. B* **2001**, *64*, 235409.
(21) Cheng, L. J.; Cai, W. S.; Shao, X. G. *Chem. Phys. Chem.* **2005**, *6*, 261.
(22) Morse, P. M. *Phys. Rev.* **1929**, *34*, 57.
(23) Doye, J. P. K.; Wales, D. J.; Berry, R. S. *J. Chem. Phys.* **1995**, *103*, 4234.
(24) Doye, J. P. K.; Wales, D. J. *J. Chem. Soc., Faraday Trans.* **1997**, *93*, 4233.
(25) Cheng, L. J.; Cai, W. S.; Shao, X. G. *Chem. Phys. Chem.* **2007**, *8*, 569.
(26) Rossi, G.; Rapallo, A.; Mottet, C.; Fortunelli, A.; Baletto, F.; Ferrando R. *Phys. Rev. Lett.* **2004**, *93*, 105503.
(27) Doye, J. P. K.; Wales, D. J. *Phys. Rev. Lett.* **2001**, *86*, 5719.
(28) Leary, R. H.; Doye, J. P. K. *Phys. Rev. E* **1999**, *60*, R6320.
(29) Cheng, L. J.; Yang, J. L. *J. Phys. Chem. A* **2007**, *111*, 2336.
(30) Roberts, C.; Johnston, R. L.; Wilson, N. T. *Theor. Chem. Acc.* **2000**, *104*, 123.
(31) Doye, J. P. K.; Leary, R. H.; Locatelli, M.; Schoen, F. *INFORMS J. Comput.* **2004**, *16*, 371.
(32) Table of the global minima of Morse clusters along with their motifs, energies, point groups, number of nearest-neighbors, strain energies, and the values of ρ_0 for which they are probably the lowest energy minimum for $81 \leq N \leq 160$ can be found in the Supporting Information. Alternatively, the table and the coordinates are available from the webpage: http://staff.ustc.edu.cn/~clj/morse/table.html.
(33) Doye, J. P. K.; Wales, D. J. *Chem. Phys. Lett.* **1995**, *247*, 339.
(34) Girifalco, L. A. *J. Phys. Chem.* **1992**, *96*, 858.